Aerodynamic Performance of Swallow Bird

H. Yusoff, M.Z. Mansor, M.R. Mat Nawi, M.Z. Abdullah, Z. Mohd Ripin and R. Ahmad

School of Mechanical Engineering, Universiti Sains Malaysia, Engineering Campus, 14300 Nibong Tebal, Penang, Malaysia.

Abstract

Aerodynamic theory and prediction provided ecologists with a useful tool for understanding the basic physics of flight, by analyzing the flow around the bird body and wings. In the present study, the experimental and simulation investigations have been made to obtain the aerodynamic performance of swallow bird (*hirundo rustica*) at different Reynolds numbers; i.e. 1.85×10^4, 4.44×10^4 and 4.81×10^4. The experimental results obtained show that the effect of feathers around bird wing have delayed the stall angle and decreased the friction drag. A 3-dimensional simulation using a Computational Fluid Dynamic (CFD) code, FLUENT 6.0 is run under same conditions as in the wind tunnel test section. The results of lift and drag coefficients from simulation results are validated with the experimental results. The simulation results have shown a fairly good agreement with the experimental results.

Keywords: Bird Flight; Reynolds Number; Lift Coefficient; Drag Coefficient; Computational Fluids Dynamics.

1. Introduction

The flight of birds is an aspect of the nature that has been paid the attention of many investigators during centuries. Large efforts have been devoted to analyze the flight of birds. Different points of view have been adopted to conduct such studies, depending on the background education and the personal interest of the scientists involved. Meseguer et al. (2003) have studied the alula effect for high lift device. The influence of the alula in the wing aerodynamics is similar to that of leading edge slats in aircraft wing, which are only operating during take-off and landing operations. Ramakrishnanda and Wong (1999) have investigated on animating bird flight using aerodynamics. They employed aerodynamic principles for the physical animation of bird flight. Hedenstrom (2003) has studied on aerodynamics, evolution and ecology of avian of flight using sophisticated techniques, has generated new and exciting insights about the evolution of flight, the function of tails and the ecological adaptations to a flying lifestyle. One of the aerodynamic advantages of bird flight is 'V' formation flying (P. Seiler et al., 2003). The theory would be confirm if it is observed that the variation in wing tip spacing is larger for birds farther form the leader than for the birds closer to the leader. Lissaman and Shollenberger (1970) have revealed that birds gain some aerodynamic advantage when in a linear formations such as the 'V', 'J' or echelon. Most of the past researchers used the wind tunnel test to investigate the aerodynamics lift and drag around wing airfoil. With the improvement of computer technology and performance, the prediction of two-dimensional and three-dimensional flow structures can be made cheaply and consumed less time for analysis. Thus, this paper presents the results of aerodynamic performance of swallow bird using experimental investigation and computational simulation. The

results of three-velocity components and pressure contours for several Reynolds number also are presented in this paper.

2. Swallow bird and wing characteristics

Swallow or scientifically named as hirundo rustica is a small perching bird found almost everywhere in the world. There are about 100 species including the martins. They are graceful flyers and can make abrupt changes a top speed in different directions because swallow has long narrow wings, forked tails, and weak feet. To analyze the flight of birds from an engineering point of view, in an extreme simplification of the problem, it can be said that birds can fly either by gliding or by flapping. The aerodynamics of wing sections is a complex problem in fluid mechanics that is satisfactorily solved at present. However, the analysis of the fluid movement around an airfoil of swallow requires both experimental testing and computer simulation for faster and cheaper technique for analysis. Those techniques are run under different Reynolds numbers and the comparison of results has been made.

Generally, the wing of a bird is similar to the human arm in many aspects. Both comprise shoulder, elbow and wrist joints followed by metacarpals (fingers) (Tricker and Tricker, 1967). The portion of the wing between the shoulder joint and the elbow joint is not aerodynamically significant for most birds and can be neglected in calculations. The cross-section of a bird's wing is quite similar to the aerofoil section of an aircraft (Houghton and Carruthers, 1982). The reader is referred to Tricker and Tricker (1967) for the anatomical details of a bird's flight muscles and to Anderson (1991) for definitions of the aerofoil parameters.

During the years 1997 and 1998, different field measurement campaigns have been carried out. Along these campaigns, several parameters of the wing geometry of almost four hundred and fifty birds, belonging to forty different species living in Spain, have been measured (the biometry method has been published elsewhere, Alvarez et al., 1997). The following parameters are used to obtain the characteristic of bird's wing.

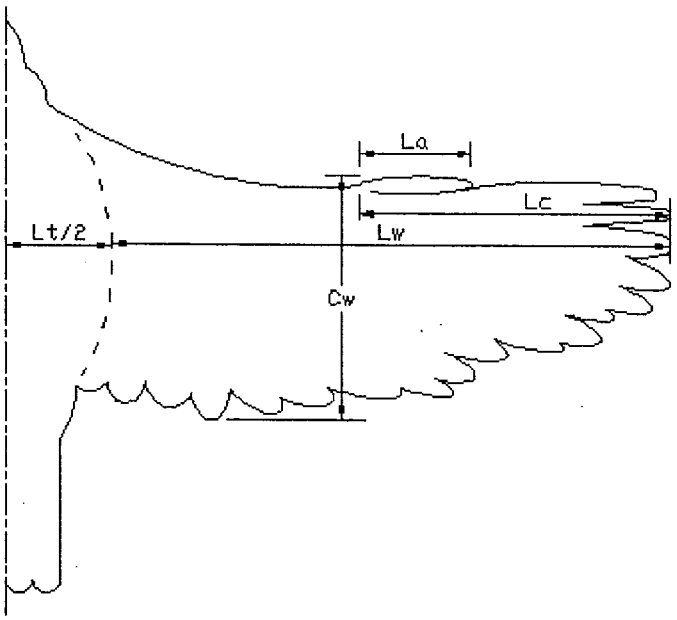

Fig. 1: Definition of the measured wing parameters

$$S_b = 2S_w + L_t c_w \qquad (1)$$

$$L_t = L_b - 2L_w \qquad (2)$$

$$W_l = Mg/S_b \qquad (3)$$

$$AR = L^2_b/S_b \qquad (4)$$

Where;

AR = aspect ratio

C_w = maximum wing chord

L_a = length of the alula

L_b = bird span

L_c = distance between the root of the alula and the wing tip

L_t = length of thorax

L_w = length of the extended wing

M = mass of the bird

S_b = total lifting surface

S_w = wing area

From these contours, the wing area, S_w and the total lifting surface of each bird S_b, have been obtained (the total lifting surface S_b has been defined according to Pennycuick (1989) , as $S_b = 2S_w + L_t c_w$, where L_t is the width of the thorax, $L_t = L_b - 2L_w$, wing load $W_l = Mg/S_b$ and to the wing geometry, the bird aspect ratio, $AR = L^2_b/S_b$). Three swallow birds have been taken as the samples in the present study in order to obtain the average values of wing load, wing area and aspect ratio (calculated in Table 1).

Table 1: Characteristics of wing shape of swallow

Number of samples	Wing Load $W_l = Mg/S_b$ (mN/cm^2)	Wing Area, S_w (cm^2)	Aspect Ratio $AR = L^2_b/S_b$
1	0.140	66.5	9.778
2	0.146	70	9.657
3	0.186	69	9.647
Average	0.157	68.5	9.694

According to the wing shapes classification proposed by Saville (1956), there are the type of wings as indicated in Table 2.

Table 2: Wing shape classification

Wing shapes classification	Function
Elliptical wing	• Wing shape is very efficient at low and moderate speeds. • Generate smooth tip vortex and uniform pressure distribution over the wing surface. • Provide good maneuverability and it is characteristic of small birds with active flight.
High speed wing	• It is characterized by low camber airfoils, moderate high aspect ratio, pronounced sweepback of the leading edge. • Wing tip is not generally slotted. • Moving in open spaces has this type of wing with high flight speeds.
High aspect ratio wing	• Typical wing of the birds that use to fly over water surfaces. • High aerodynamic efficiency and could be labeled also high speed soaring wings.
High lift wing	• Characterized by slotted wing tip, moderate aspect ratio and pronounced camber airfoils. • Very efficient at low speeds and they seems to be especially adapted for soaring flight over the land.

	• This wing could be also described as low speed soaring wings.

3. Experimental Set-up

The experiment has been carried out in a low speed and open circuit wind tunnel (Figure 2). The wind tunnel has a 300 mm x 300 mm x 600 mm Plexiglas test section with three components electronic balancing unit for the measurement of lift, drag and turning moment. A preserved swallow bird with the feathers on has been located in the middle of the test section. The velocity in the wind tunnel has been measured by using Pitot tube. The maximum velocity in the test section is 38 m/s. The test was conducted at two different Reynolds numbers of 44000 and 48000. The swallow bird has been rotated at different angles of attack from 36° to -36°.

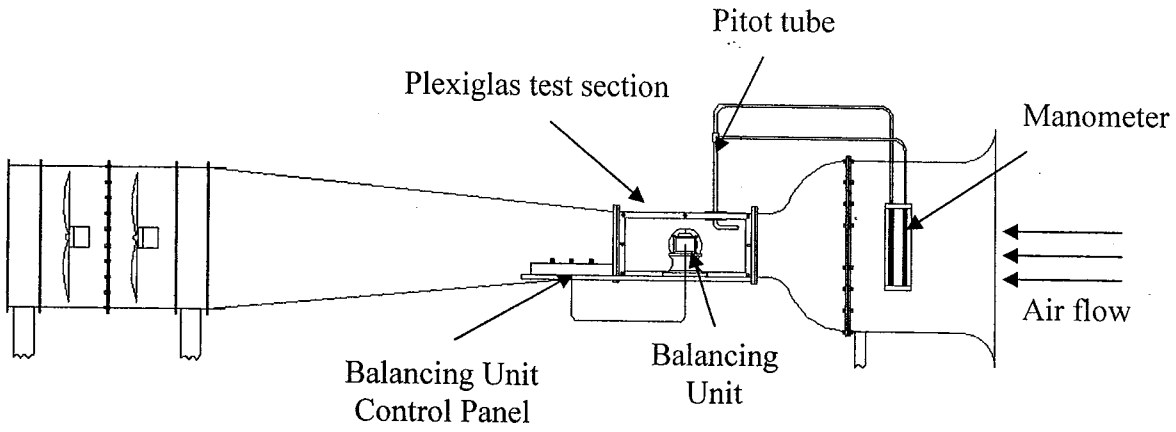

Figure 2: Low speed open circuit wind tunnel

3.1 Formulation and simulation setup

The steady flow of a viscous incompressible fluid flow around a swallow bird is considered. The basic equations used in the simulation are the equation of continuity and the Navier-Stokes equations:

$$\vec{\nabla} \cdot \vec{V} = 0 \tag{5}$$

$$(\vec{V} \cdot \vec{\nabla})\vec{V} = -\frac{1}{\rho}\vec{\nabla}P + \nu\nabla^2\vec{V} \tag{6}$$

where $\vec{\nabla} = \frac{\partial}{\partial x} + \frac{\partial}{\partial y} + \frac{\partial}{\partial z}$

CFD software FLUENT 6.0 and the pre-processor software GAMBIT 1.2 are used in the investigation to predict the lift and drag coefficients. The simulation followed the same condition as in wind tunnel. Unstructured meshes are used to model a swallow bird without considering its' feathers to avoid complexity in the modeling. In meshing process, the need to reduce the time required to design and develop a configuration often required the users to obtain solution on computational meshes that are relatively small although computer's speeds and memory sizes have increased, allowing the solution of larger flow problem as proposed by Van Dam (1999). For the turbulence analysis, the k-ε model is used in the investigation. The mesh generated around a swallow bird as shown in Figure 3.

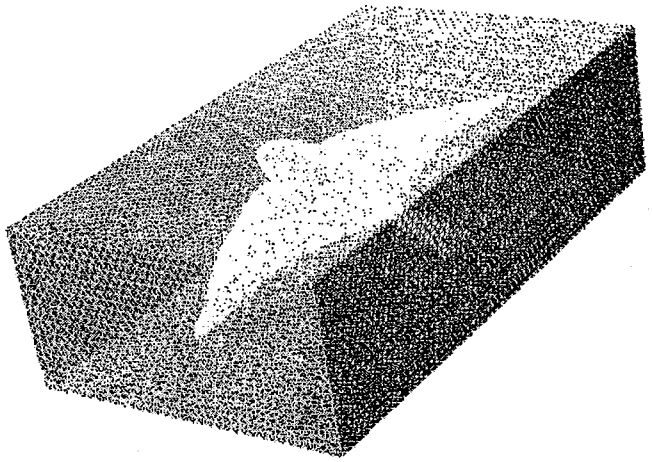

Figure 3: Mesh around swallow bird

The k-ε turbulence model is used in order model the turbulence. The equations describing the relationship between turbulence intensity and turbulence kinetic energy, k and turbulence dissipation rate, ε as follow:

$$k = \frac{3}{2}(U \times TI)^2 \qquad (7)$$

$$\varepsilon = C_{\mu}^{\frac{3}{4}} \frac{k^{\frac{3}{2}}}{l} \qquad (8)$$

where $C_{\mu} = 0.09$

l = turbulence length scale $\approx 0.07C_w$

C_w = maximum wing chord

U = free stream velocity

TI = turbulence intensity

The maximum wing chord is taken as the characteristic length, C_w.

4. Results and Discussion

4.1 Experimental Results

The experiments have been carried out at two different Reynolds numbers; i.e. 4.44×10^4 and 4.81×10^4. The experiment has been made at various angles of attack from -36° to 36°. The results presented are lift, drag, drag polar and lift to drag ratio curves.

The results obtained for the lift coefficients of the swallow in the wind tunnel under two Reynolds numbers are shown in Figure 4. The profile shows that the lift coefficient is increased when the angle of attack increases. This increment is continuous until the angle of attack reaches the stall angle. After that, the lift coefficient is reduced. The results obtained show similar trends for common airfoil or aircraft wings. At $\alpha = 0$, the C_L is 0.14 for $Re = 4.4 \times 10^4$ and 0.13 for $Re = 4.81 \times 10^4$. The maximum lift coefficient, C_{Lmax} is occurred at $\alpha = 32°$. This stall angle is higher (delayed) compared to the common aircraft wing around 12-20°. One of the reasons may be due the effect of feathers around the swallow bird. The C_{Lmax} for $Re = 4.44 \times 10^4$ is 0.97 and for the $Re = 4.81 \times 10^4$, the C_{Lmax} is 0.93. Up to $\alpha = 36°$, the lift coefficient suddenly decreased. The lift coefficient decreases approximately 5.15% ($Re = 4.44 \times 10^4$) and 8.6% ($Re = 4.81 \times 10^4$) lower than the maximum lift coefficient.

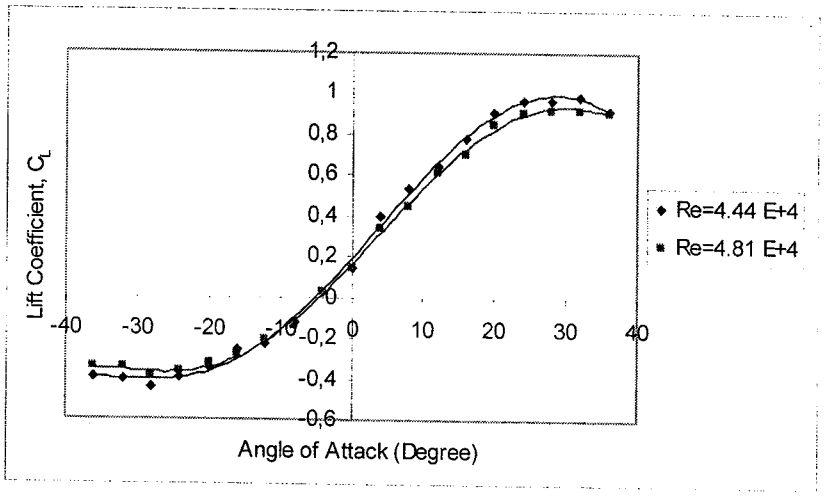

Figure 4: Lift curve obtained from experiment

Figure 5 shows the drag coefficient against the angle of attack. The results indicate that the drag coefficient is increased gradually with the angle of attack increases where the trends of the result like as a 'V' shape. After the stall angle, the drag coefficient is slightly increased. Between $\alpha = 5^\circ$ to $\alpha = -5^\circ$, the drag coefficient decreases up to the stall angle ($\alpha = 26^\circ$). After the stall, the drag coefficient increased about 21.8% and 20.4% for Re = 4.4 x 10^4 and Re = 4.81 x 10^4 respectively.

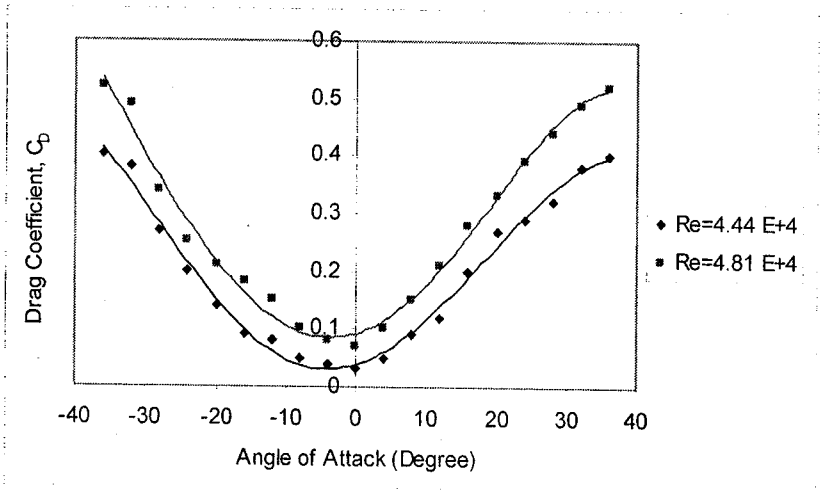

Figure 5: Drag curve obtained from experiment

The drag polar for the two Reynolds numbers is presented in Figure 5. It indicates that the C_{Lmax} = 1 at C_D = 0.33 for Re = 4.4 x 10^4 and C_{Lmax} = 0.88 at C_D = 0.45 for Re = 4.81 x 10^4. Drag polar characteristic is important to describe the aerodynamic performance.

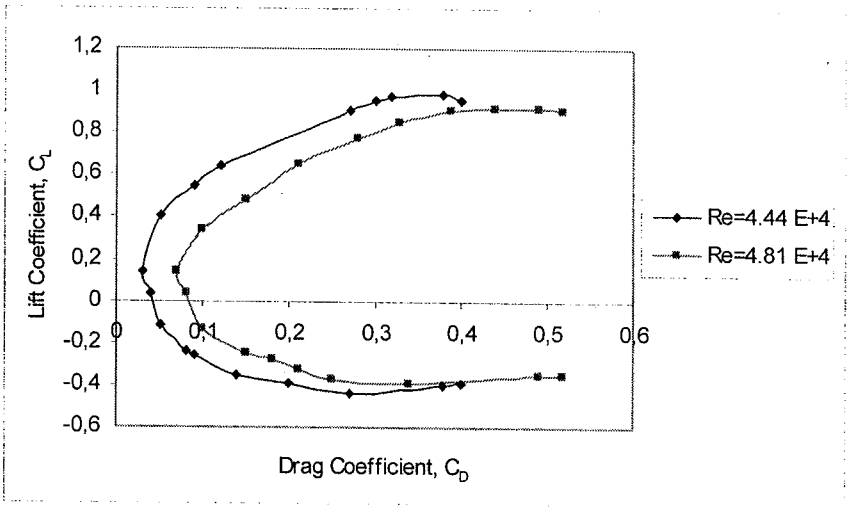

Figure 6: Drag polar curve

The relation between lift to drag ratio and angle of attack for two different Reynolds numbers is shown in Figure 7. The aerodynamic efficiency of swallow bird model can be measured by referring to Figure 7. For the aircraft design, lift to drag ratio is an important parameter to obtain the most suitable thrust required at a ranging Reynolds number. The minimum thrust required at certain velocity is at maximum L/D. In Figure 7, all curves show a similar trend. Generally, the L/D ratios increase at $\alpha = 0°$ to $\alpha = 4°$ and after that, the L/D ratio is decreased. The highest value of L/D ratio is 8 at $\alpha = 4°$ for Re 4.81 x 10^4.

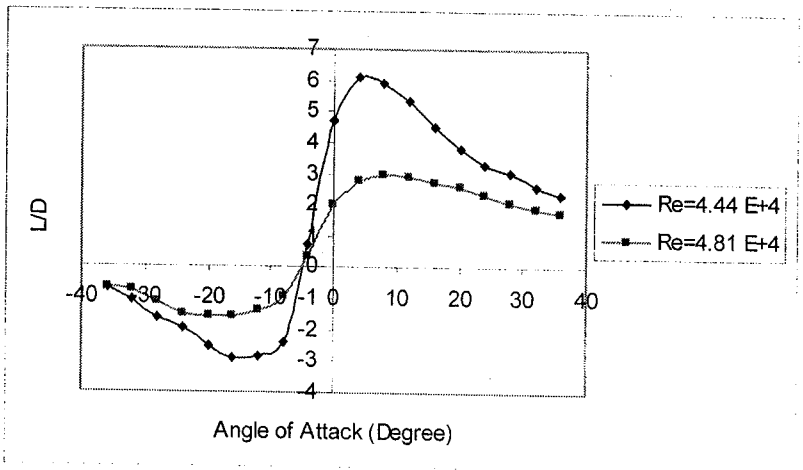

Figure 7: Lift to drag ratio curve

Effect of Reynolds numbers on the aerodynamic lift and drag coefficient are shown in Figures 8 and 9. In Figure 8, the result indicates that positive lift coefficients, $+C_L$ and negative lift coefficients, $-C_L$ are decreased with Reynolds number increases. However, the variation of C_L is very small. At $\alpha = 28°$ (stall angle) between Re = 4.44 x 10^4 and Re = 4.81 x 10^4, the difference of C_L is approximately 5.43%.

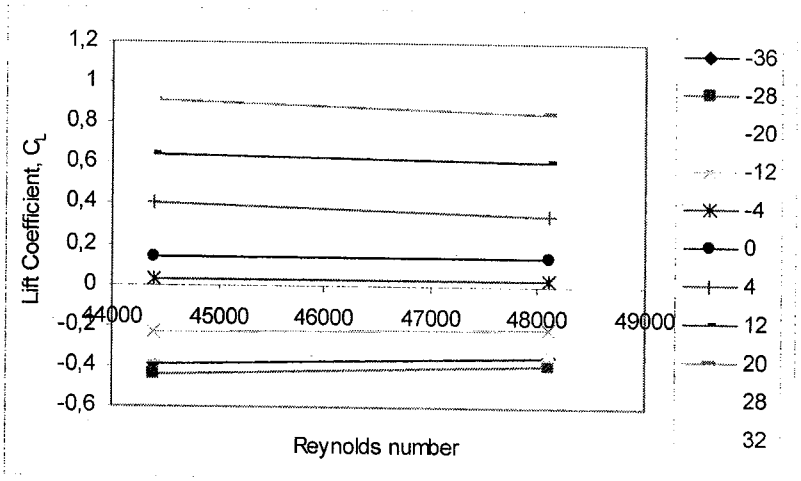

Figure 8: Effect of Reynolds numbers on lift coefficients

Figure 9 shows the drag coefficient against Reynolds numbers. The trend shows the difference of C_L is wide at higher angle of attack approximately from -12° to -36° and 12° to 36° meanwhile at smaller angle of attack approximately from -11° to 11°, the difference of C_L is small. At α = 28° (stall angle), the difference of drag coefficient, C_D between Re = 4.44 x 10^4 and Re = 4.81 x 10^4 is about 37.5%.

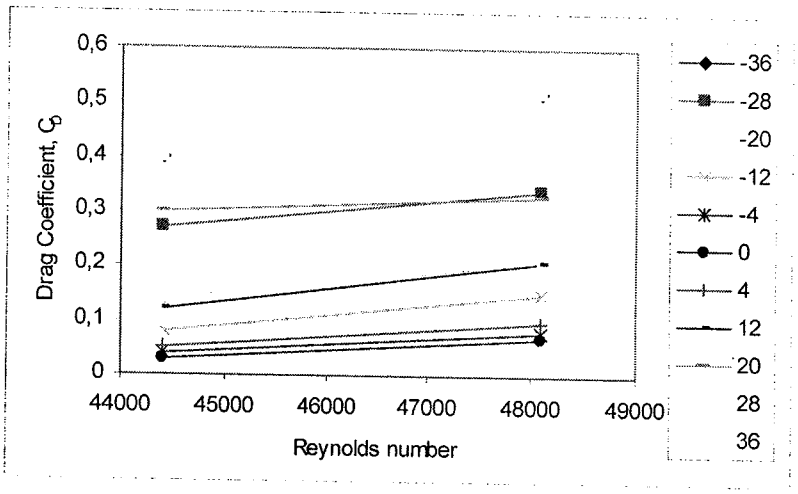

Figure 9: Effect of Reynolds numbers on drag coefficients

4.2 Simulation results

Three dimensional flow simulations around swallow bird have been made at three different Reynolds numbers i.e. 1.85 x 10^4, 4.44 x 10^4 and 4.81 x 10^4. Figures 10 to 11 show the results for the lift and drag coefficients at different Reynolds numbers and angle of attacks of α = -34° to α = 32°. Figure 10 indicates that lift coefficients is increased when the angle of attacks increases and the highest C_L is occurred at Re = 1.85 x 10^4. The C_L values almost same for the three Reynolds numbers and the variation occurs when α reaches 20° and above. At α = 0°, the C_L approximately -1.024, -0.110 and -0.110 for Re = 1.85 x 10^4, Re = 4.44 x 10^4 and Re

= 4.81 x 10^4 respectively. At α = 32°, the lift coefficient is approximately 1.014, 0.839, 0.828 for Re = 1.85 x 10^4, 4.44 x 10^4 and 4.81 x 10^4 respectively. The stall phenomenon could not be observed as observed in the experiment due to limitation of the turbulence model used.

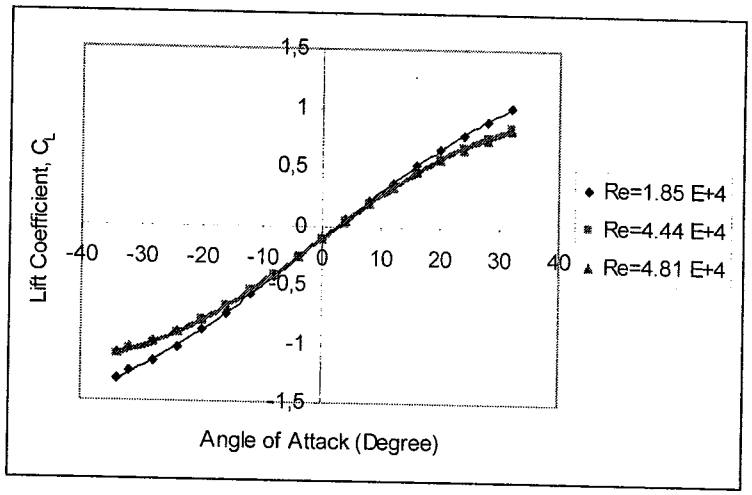

Figure 10: Simulation lift curve at Re = 1.85 x 10^4, 4.44 x 10^4 and 4.81 x 10^4

Figure 11 shows the drag coefficients against angles of attack at different Reynolds numbers. The result shows that the lowest drag coefficient is at Re = 4.81 x 10^4. The graph shows that C_D is increased when the angle of attack increases. At Re = 1.85 x 10^4, the highest value of C_D is 0.756 and at α = 32°.

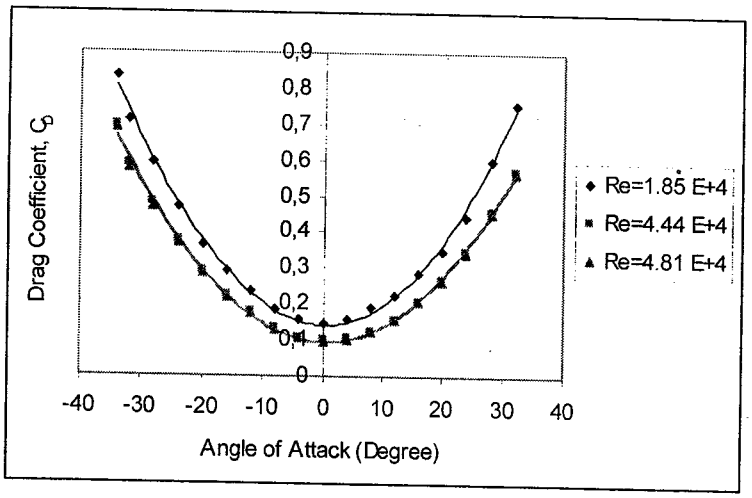

Figure 11: Simulation drag curve at Re = 1.85×10^4, 4.44×10^4 and 4.81×10^4

4.3 Pressure contour and velocity vector

In the simulation, two parameters have been considered; i.e. pressure contour and velocity vector. In pressure contour, the result shows the general pressure distribution around the body and wings of swallow bird when it is subjected to a certain angle of attack and different Reynolds numbers. Generally, pressure contour indicates that the highest pressure is occurs at the beak of the bird locating in front of the body. The pressure also high at the wing leading edge, but the pressure is low at the wing tip. At the upper surface of the body and wing, the pressure is lower compared to the front and lower of the body surfaces.

The study on pressure contour is based on three different of angles of attack; α= -8, 0°, and 8° and at Reynolds number of 4.44×10^4 as shown in Figures 12 through 14. In Figure 12, it shows at angle of attack below than zero (α = -8°), the stagnation point located at the upper surface of the swallow beak. The pressure at the upper surface is higher than the lower surface of the bird. At the wing tip, the pressure becomes lower because the air moves faster on that surface. The highest pressure at the upper surface of the wing is about 41% compared to the upper surface in Figure 13 (α = 0°). The lowest pressure is about 2.46×10^2 Pa occurred at the lower surface of the bird's central body. Meanwhile, the highest pressure (about -1.35×10^2Pa) is occurred at the lower part of body and wing.

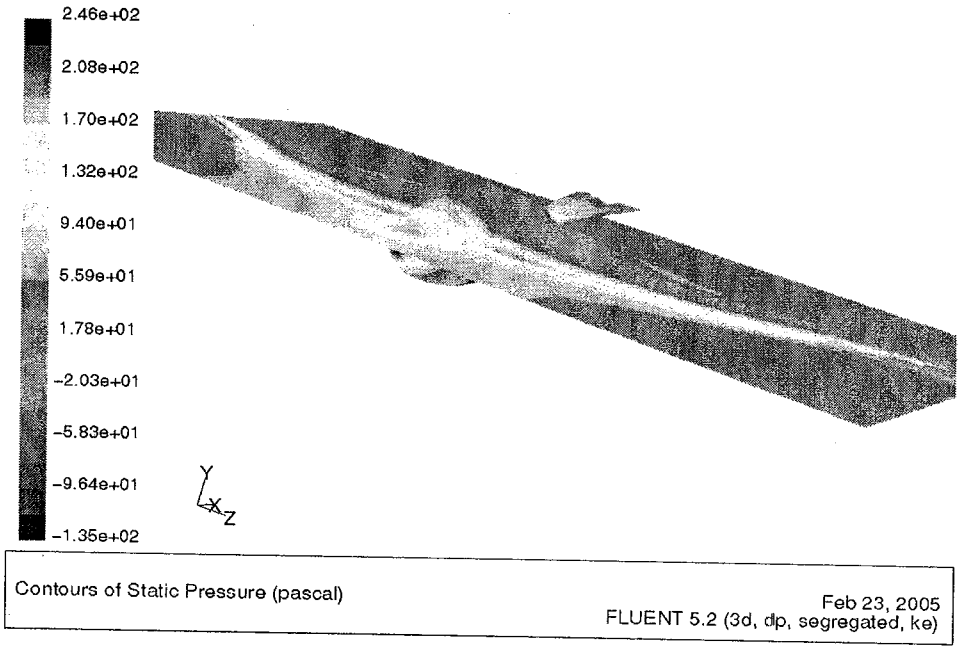

Figure 12: Pressure contour at $\alpha = -8°$

Pressure contour around swallow bird at $\alpha = 0°$ is shown Figure 12. At this condition, the flow is moving parallel to the swallow bird body and wings. In this figure, the contour illustrates that the highest pressure (about 2.41×10^2 Pa) is occurred at the center of swallow's beak and also at the leading edge of the wing. At the lower surface and the wing tip, the pressure is low. The lowest pressure region is located at the wing upper surface near the body and the pressure is about -6.41×10^2Pa. As comparison, the pressure at the upper surface of swallow at $\alpha = -8°$ (in Figure 12) is lower (about 70%) compared to the upper surface of swallow at $\alpha = 0°$ (Figure 13). It is shown pressure on the upper surface is decreased with the angles of attack increases.

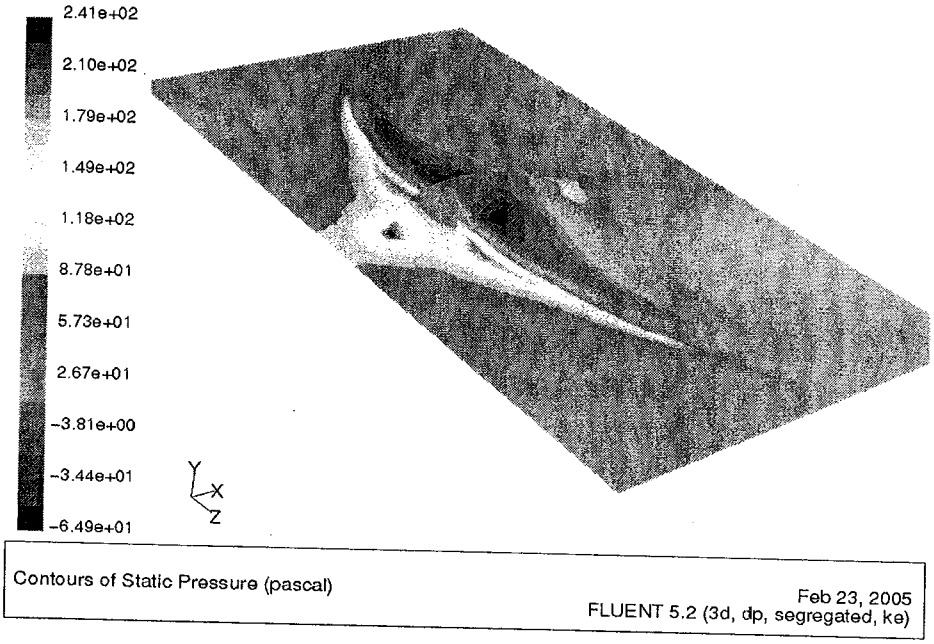

Figure 13: Pressure contour at $\alpha = 0°$

For the case $\alpha = 8°$ as shown in Figure 14, the stagnation point move backward to the lower surface and the highest pressure region is growing. At the upper surface of swallow bird, the pressure is lower (about 34%) compared to the Figure 13 ($\alpha = 0°$). At $\alpha = 8°$, the highest pressure (about 2.51×10^2 Pa) is occured at beak and at the wing leading edge whereas the lowest pressure region approximately -1.35×10^2 Pa is located at the wing upper surface near the body.

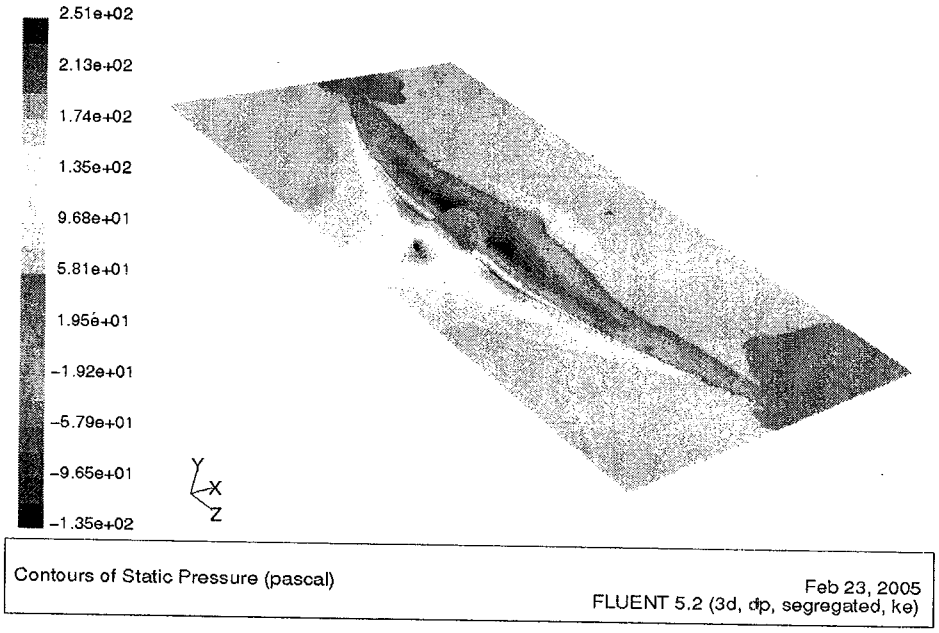

Figure 14: Pressure contour at $\alpha = 8°$

Again for the velocity vector around swallow bird at three different angles of attacks; i.e. $\alpha = -8°$, $0°$ and $8°$ are shown in Figures 15 through 17. At $\alpha = -8°$ (in Figure 15), the velocity is higher about 14.4 m/s at the upper surface of swallow bird. At the bird beak (stagnation point) and the leading edge of the wings, the velocity is low about 6.61 m/s. The velocity is high at the lower surface and wing tip of the swallow bird. The highest velocity is observed at the mid section of the lower surface wing. This highest velocity is increased about 29% compared to the free stream velocity.

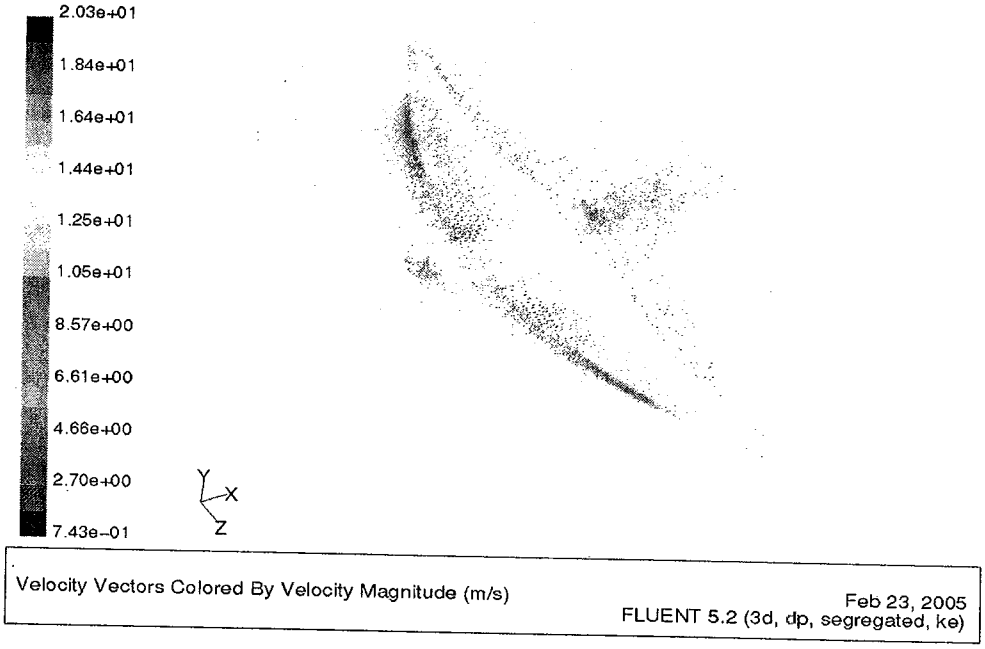

Figure 15: Velocity vector at $\alpha = -8°$

Figure 16 presents the velocity vector around swallow bird at $\alpha = 0°$. At this angle, the flow is moving parallel to the swallow bird body and wings. So, the highest velocity is occurred at the mid of upper surface of the wings. This figure also shows the velocity of the flow is low about 6.43 m/s at the peak (stagnation point) and at the leading edge. The value of the highest velocity is about 2% increases from the free stream velocity.

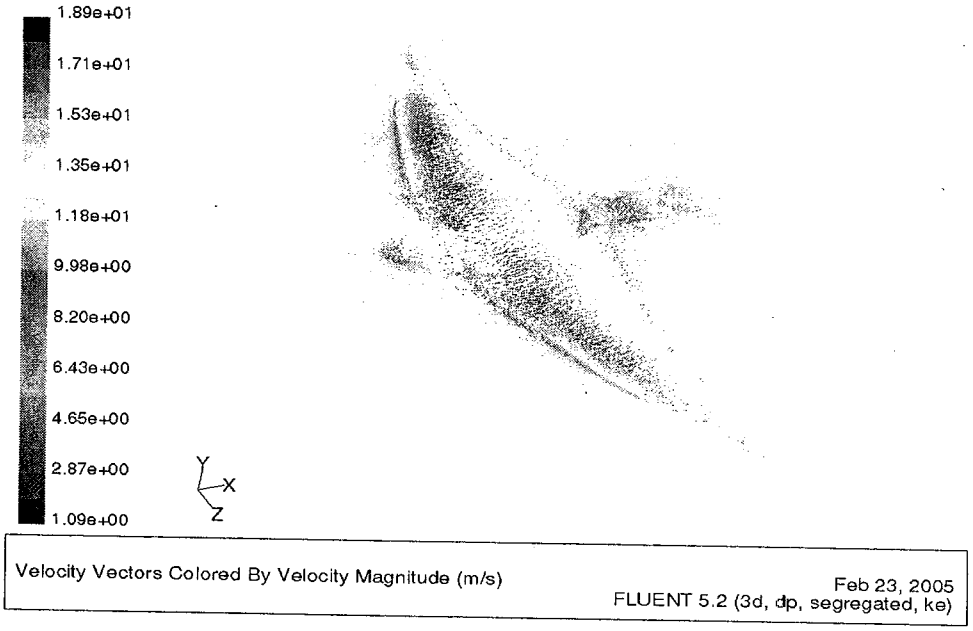

Figure 16: Velocity vector at $\alpha = 0°$

For the swallow at $\alpha = 8°$ (Figure 17), the stagnation point moves backward to the lower surface. At the lower surface and the leading edge wing, the velocity is low about 7.1 m/s. The lowest velocity (about 2.0 m/s) occurs at between body and tail, meanwhile the highest velocity (about 20 m/s) occurs at the mid of upper surface wing. The highest velocity value is increased about 38% compare to the free stream velocity.

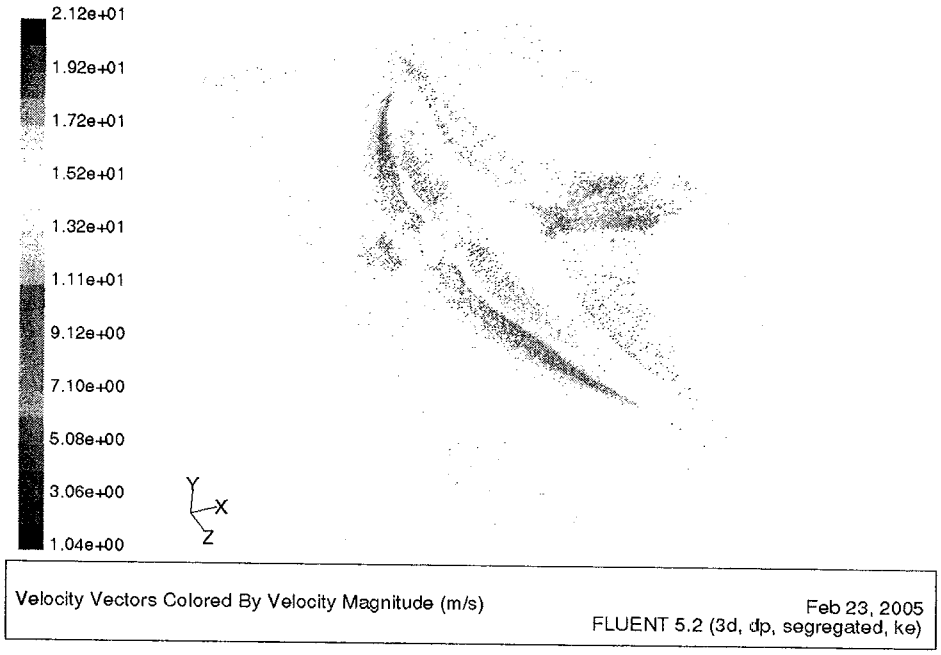

Figure 17: Velocity vector at $\alpha = 8°$

4.4 Comparison between experimental and simulation results

Figures 18 through 21 are presented the comparison between the experimental and computational simulation results. The comparison is made at Re = 4.44×10^4. Figure 18 shows the comparison results of lift coefficient, C_L. Two curves, experimental and simulation results show a similar trend. The trend shows the value of C_L is increased when the angle of attack increasing. But, the C_L is immediately decreased after the stall angle for the experimental result. The C_L maximum is 0.97 at $\alpha = 28°$. Figure 18 shows the lifts slope for experimental results are 0.028 per degree and 0.031 per degree for simulation result. The value of simulation result predicted about 9.6 % lower than the experimental result. The difference occurs due to the effect of swallow feather gave higher lift coefficient for experimental results, whereas

in the simulation, the bird with no feathers is used. However, the simulation results are shown still fairly good agreement with the experimental results.

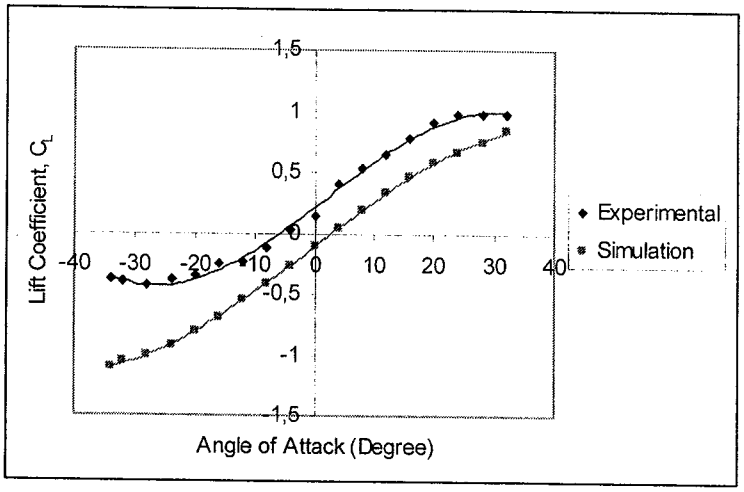

Figure 18: The lift curve at Re = 4.44 x 10^4

The comparison results for drag between simulation and experimental are shown in Figure 19. The pattern shows of the two graphs are similar trends. The experimental drag curve is lower than the simulation drag curve. The drag slope for simulation result is 0.016 per degree while 0.013 per degree for experimental result. In average, the experimental result is about 18% lower than the simulation results. The simulation and experimental results are shown in good agreement. Again the differences due to the effect of swallow feathers in the experimental results have delayed the separation and reduce drag friction coefficient.

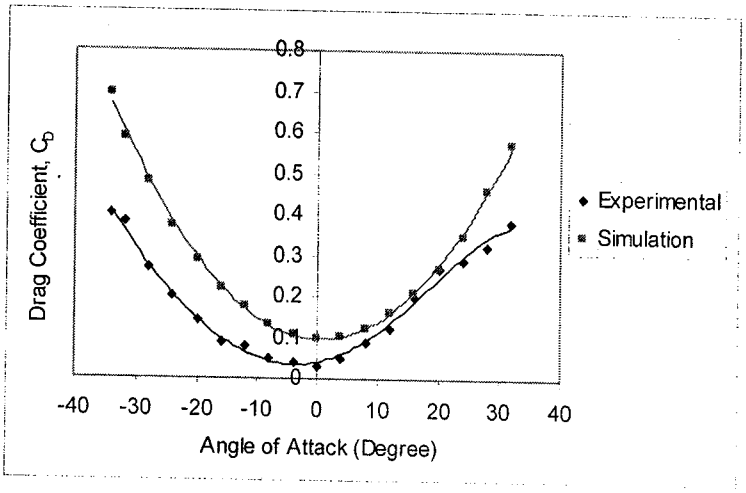

Figure 19: The drag curve at Re = 4.44 x 10^4

The comparison results are continued for lift to drag ratio against angle of attack as shown in Figure 20. Both curves have shown a similar trend. The experimental curve is higher than the simulation curve. From experimental results, the maximum L/D ratio is 4.6 at $\alpha = 12°$ while the highest L/D ratio for simulation results is 2.1 at $\alpha = 18°$. The maximum L/D ratio for simulation is about 50% lower than the experimental result.

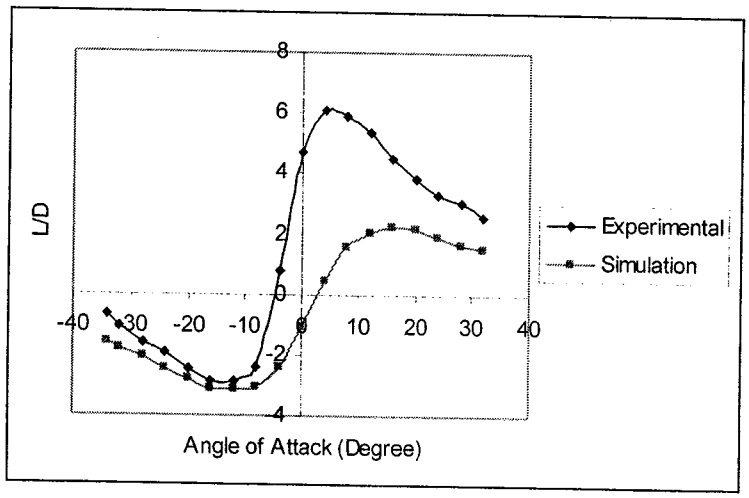

Figure 20: The lift to drag ratio curve at Re = 4.44 x 10^4

The comparison of drag polar curve between experimental and simulation results are shown in Figure 21. It indicated that drag polar from experiment is higher than simulation. The highest C_L value for experiment is 0.97 and 0.8 is the highest C_L for simulation. The difference between these two maximum values is about 18 %.

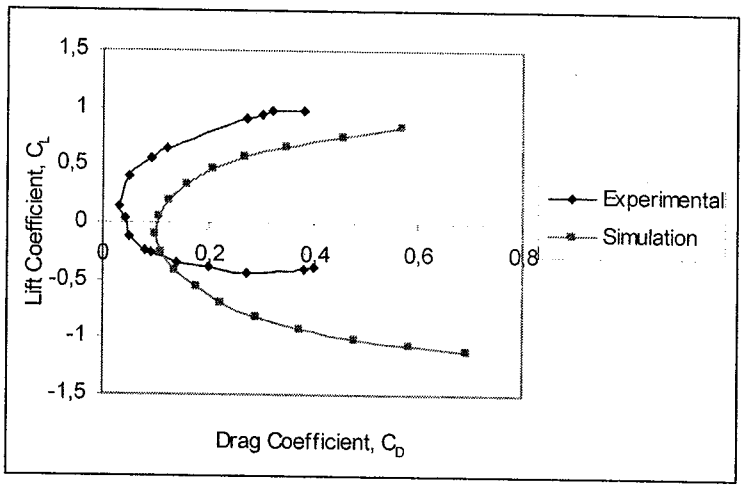

Figure 21: The drag polar curve at Re = 4.44 x 10^4

5. Conclusion

In this study, the aerodynamic characteristic of swallow bird has been investigated by using a wind tunnel experiment and computer simulation. The experimental investigation is made in order to validate the simulation results. However, the simulation results are limited due to the swallow model has made with no feathers attached. Generally, both experimental and simulation results show the lift and drag coefficients are increased with the angle of attack increases.

In simulation study, the stall phenomenon could not be observed due to limitation in the k-ε model as described other workers. It also found the effect of Reynolds numbers on the aerodynamic characteristic is too small. The contours

illustrate that high velocity and low pressure are occurred at the upper wing and wing tip meanwhile the parts like beak, trailing and leading edge, lower wing and also tails have low velocity and high pressure in nature.

The comparison between simulation and experimental results are shown fairly agreement. The lift coefficient of experimental is higher than the simulation. However, the drag coefficient of experimental is lower compared to the simulation. The differences due to the swallow with feathers are considered in the experiment has increased the lift coefficient, reduced the drag friction coefficient and also delayed the stall. As a result, the experimental results of lift to drag ratio and drag polar show a higher value compared to the simulation.

Nomenclature

AR	aspect ratio
C_D	drag coefficient
C_L	lift coefficient
C_{Lmax}	maximum lift coefficient
C_w	maximum wing chord (cm)
d	the interval size
k	kinetic energy of turbulence
l	turbulence length scale
L_a	length of the alula (cm)
L_b	bird span (cm)

Acknowledgements

The authors wish to thanks the Universiti Sains Malaysia and the Ministry of Higher Education of Malaysia for their financial supports under the Fundamental Research Grant.

References

Anderson, J.D. (1991). 'Fundamentals of Aerodynamics'. (McGraw-Hill: New York.)

Alvarez, J.C., Perez, A. and Meseguer, J. (1998). Biometria de la pardela cenicienta calonectris diomedea y paino comun Hydrobates Pelagius, in Anuari Ornitologic de les Balears 1997 Volum 12 (in Spanish), pp. 17-28.

Hedenström, A. (2003). Flying with holey wings. *Journal of Avian Biology*, Vol. **34** Issue **4**, 324-327.

Houghton, E.L., Carruthers, N.B. (1982). 'Aerodynamics for Engineering Students. (Arnolds: London.)

J. Meseguer, J.C. Alvarez, E. Meseguer, A. Perez (2003). The alula: a leading edge, high lift device of birds. (IDR/UPM, E.T.S.I. Aeronauticos, Universidad Politecnica de Madrid.)

Lissaman, P., Shollenberger, C. (1970). Formation flight of birds. Science **168**, 1003-1005.

P. Seiler, A. Pant, J.K. Herdick (2003). A systems interpretation for observations of bird V-formations. *Journal of Theoretical Biology* **221**, 279-287.